Wind Tunnel Study of Turbulent Flow Structure in the Convective Boundary Layer Capped by a Temperature Inversion

EVGENI FEDOROVICH, ROLF KAISER, MATTHIAS RAU, AND ERICH PLATE

Institut für Hydrologie und Wasserwirtschaft, Universität Karlsruhe, Karlsruhe, Germany

(Manuscript received 1 March 1995, in final form 3 October 1995)

ABSTRACT

Experiments on simulating the atmospheric convective boundary layer (CBL), capped by a temperature inversion and affected by surface shear, were carried out in the thermally stratified wind tunnel of the Institute of Hydrology and Water Resources, University of Karlsruhe. The tunnel is of the closed-circuit type, with a test section 10 m long, 1.5 m wide, and 1.5 m high. The return section of the tunnel is subdivided into 10 layers, each driven by its own fan and heating system. By this means, velocity and temperature profiles can be preshaped at the inlet of the test section, which allows for the reproduction of developed CBL over comparatively short fetches. The bottom heating is controlled to produce the constant heat flux through the floor of the test section. The flow velocity components in the tunnel are measured with a laser Doppler system; for temperature measurements, the resistance-wire technique is employed.

A quasi-stationary, horizontally evolving CBL was reproduced in the tunnel, with convective Richardson numbers $\mathrm{Ri}_{\Delta T}$ and Ri_N up to 10 and 20, respectively, and the shear/buoyancy dynamic ratio u_*/w_* in the range of 0.2–0.5. Within the employed modeling approach, means and other statistics of the flow were calculated by temporal averaging. Deardorff mixed-layer scaling was used as a framework for processing and interpreting the experimental results. The comparison of the wind tunnel data with results of atmospheric, water tank, and numerical studies of the CBL shows the crucial dependence of the turbulence statistics in the upper part of the layer on the parameters of entrainment, as well as the modification of the CBL turbulence regime by the surface shear.

1. Introduction

The convective boundary layer (CBL) commonly develops in the atmosphere during fair weather days, when convective heat transfer from the warm ground surface acts as the main turbulent forcing. Wind shears at the surface and across the interfacial or entrainment layer, located at the top of the CBL, also contribute to turbulence generation. In many instances the buoyant production of turbulence in the CBL dominates the mechanical one, and the convection can be taken as shear free. This particular case of CBL has been subject to thorough experimental studies both in nature and in the laboratory, whereas only limited experimental information is available about the CBL with shear. This type of CBL cannot be reproduced easily using laboratory facilities. Effects of the wind shear in the atmospheric CBL are usually camouflaged by other nonconvective forcings.

Among the field studies of the CBL, those of Clarke et al. (1971), Kaimal et al. (1976), Caughey and Palmer (1979), and Lenschow et al. (1980) should be mentioned. Data from their measurements are widely used to verify models and parameterizations of the CBL. However, the comparative analysis of atmospheric data with results of water tank and large eddy simulations (LES) of the CBL, given, for instance, in Schmidt and Schumann (1989), Sorbjan (1991), and Fedorovich and Mironov (1995), shows that the interpretation of field data is severely handicapped by the combined effect of wind shear, advection, large-scale subsidence, and gravity waves on the turbulence regime of the atmospheric CBL. When turbulence statistics from atmospheric measurements are plotted using Deardorff (1970) mixed-layer scales, they display a considerable scatter and in many cases also systematic shifts with respect to CBL turbulence data from other sources.

Water tank simulations of the CBL give a method of investigation of the pure case of the shear-free, horizontally quasi-homogeneous CBL. Despite limitations, arising from the influence of tank geometry and questionable comparability with atmospheric data due to lower values of Reynolds and Rayleigh numbers (Sorbjan 1991), experiments in tanks continue to be the most reliable source of information on the turbulence structure of buoyancy-driven boundary layers. The classic water tank simulations of the CBL have been per-

Corresponding author address: Dr. E. Fedorovich, Institut für Hydrologie und Wasserwirtschaft, Universität Karlsruhe, Kaiserstraße 12, 76128 Karlsruhe, Germany.
E-mail: gg07@dkauni2.bitnet

formed by Deardorff et al. (1969, 1980), Willis and Deardorff (1974), and Deardorff and Willis (1985). They comprehensively studied turbulence statistics and spectra in the shear-free CBL. Kumar and Adrian (1986) complemented these studies by detailed measurements of higher-order turbulence moments in the entrainment layer. The turbulent regime with nonpenetrative convection was investigated in a tank by Adrian et al. (1986). Recently, the water tank simulations of turbulent convection in the atmospheric boundary layer have been performed by Cenedese and Querzoli (1994). Their data generally agree with the results of Deardorff et al.

Wind tunnel simulations of the CBL have not been as extensive. Actually, very few wind tunnel studies of the CBL have been reported in the literature. Discussing the operating ranges of the wind tunnels for the simulation of the CBL, Meroney and Melbourne (1992) present a list of currently existing facilities capable of reproducing CBL phenomena. Being rather sophisticated and delicate tools, the majority of these installations are still under construction and evaluation. Systematic studies intended to simulate the atmospheric CBL flow have been carried out so far only in three thermally stratified wind tunnels: at the Ecole Centrale de Lyon (Rey et al. 1979), at Japan's National Institute for Environmental Studies (NIES), (Ogawa et al. 1980), and at the Colorado State University (CSU, Poreh and Cermak 1984).

The investigations of Rey et al. (1979) were focused on the development of convection in a neutrally stratified flow passing over a heated plate with smooth or rough surface. The capping effects of stable stratification were not considered for technical reasons. In this way, the attempt was made to simulate the atmospheric surface layer under convective conditions. The observed discrepancies between the wind tunnel and atmospheric data with respect to velocity components variances, kinetic energy dissipation rate, and turbulence spectra Rey et al. (1979) explained by smaller values of the Reynolds number in the tunnel flow.

The NIES team investigated several cases of the CBL developing over the heated surface. In the seabreeze simulation, the floor of the first half of the test section was cooled to establish the stable stratification, which was eroded downstream by the internal CBL growing over the heated second half of the floor. Close inspection of the velocity and temperature profiles from Ogawa et al. (1980) makes evident that the experimental setup chosen was not sufficient to clearly represent the effects of capping temperature inversion and to appropriately resolve the structure of turbulent layer, which appeared to be very shallow in the case studied. We do not know of any other measurements in the NIES tunnel relevant to flow configurations characteristic of the atmospheric CBL.

A similar cooling–heating scheme CBL is applied in the wind tunnel of CSU, which was used for studies of diffusion in the CBL environment. The CBL turbulence structure was not a subject of these studies. Only mean-flow characteristics in the simulated CBL are presented, for instance, in Poreh and Cermak (1984). These characteristics can be used for a rough evaluation of the convective regime reproduced in the tunnel. Such an evaluation, supplemented with analysis by Meroney and Melbourne (1992), allows one to conclude that the method of CBL generation employed in the CSU tunnel imposes serious limitations on operating ranges with respect to a number of important integral parameters of the CBL, namely, the inversion strength, the boundary-layer depth, the temperature gradient in the turbulence-free layer, and the surface heat flux. The crucial problem of the cooling–heating approach is the necessity to have a very long test section in order to simulate a sufficiently deep CBL.

Our experience of operating the thermally stratified wind tunnel at the Institute of Hydrology and Water Resources (IHW), Karlsruhe University, shows that some of the above problems can be reduced if design of the tunnel allows preshaping profiles of mean-flow characteristics at the test section inlet. Such preshaping implies that general features of the CBL mean-flow structure are known, and therefore in the upstream flow the configuration roughly corresponding to the developed CBL can be prescribed. The preshaped flow proceeds downstream over the heated floor of the tunnel, with convective turbulence penetrating into the flow and adjusting its mean structure to a local turbulent regime. This gives an opportunity to generate a deep CBL over a comparatively short fetch. By varying the initial temperature and velocity profiles, different forcings affecting the turbulence regime in the CBL can be investigated, for instance, effects of shear omitted in water tank CBL simulations.

The concept of the stratified tunnel of IHW has been given in Rau et al. (1991) and will be summarized in section 2 of our paper. Comprehensive tests to evaluate the tunnel for modeling atmospheric convection were performed within the last several years. Operating ranges of the tunnel with respect to different parameters of the flow were established, and similarity requirements for relating the model CBL to its atmospheric prototype were determined. These methodical studies are reviewed in Poreh et al. (1991) and Rau and Plate (1994).

In the present paper for the first time we show wind tunnel results from experiments on simulating the atmospheric boundary layer with convection. For comparing measured turbulence characteristics with data from other experimental CBL studies, most of which dealt with the shear-free convection, we focus primarily on flow configurations characterized by a moderate influence of the wind shear. Mean velocity and temperature profiles are demonstrated as well. The wind tunnel experiments to be presented can be considered as a source of independent data on the CBL and tur-

bulence structure, complementing existing datasets from field measurements, water tank modeling, and LESs of atmospheric convection.

The experimental setup employed, and the apparatus used to measure velocity and temperature will be described in section 2, where the technique of flow visualization is also considered and an interpretation of two visualized patterns is given. Section 3 contains results of measurements of mean-flow characteristics. Turbulence statistics are shown and analyzed in section 4. In section 5 the wind tunnel results are compared with atmospheric, water tank, and LES data. Section 6 summarizes the conclusions.

2. Experimental setup

a. Design of the thermally stratified wind tunnel

The wind tunnel of IHW is specially designed for simulating typical convective conditions in the lower atmosphere, where a convectively mixed layer developing over a heated surface is capped by a temperature inversion. The tunnel is of the closed-circuit type, with a test section 10 m long, 1.5 m wide, and 1.5 m high. The return section of the tunnel is subdivided into 10 layers, which are individually insulated. Each layer is 15 cm deep and driven by its own fan and heating system. With this design, the velocity and temperature vertical distributions can be preshaped at the inlet of the test section (see Fig. 1). By means of a feedback control system, various disturbances in the flow are compensated for while it passes through the return section, and steady-state conditions in the flow entering the test section are provided. The floor of the test section, which is constructed of smooth aluminium plates, is also heated, with energy input controlled to produce a constant heat flux.

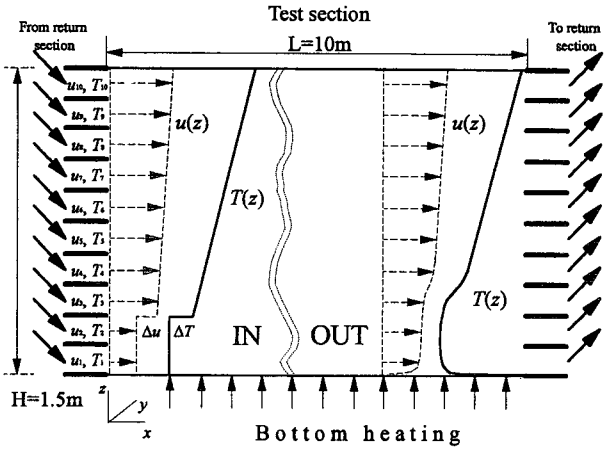

FIG. 1. Scheme of simulating the atmospheric CBL in the thermally stratified wind tunnel of IHW.

b. Measurement and visualization technique

The components of flow velocity in the tunnel are measured with a laser Doppler velocimeter (LDV), which allows single-point velocity measurements of high accuracy. The ellipsoidal measuring volume has a typical diameter of 0.16 mm and a length of 2.84 mm. The independence with respect to temperature fluctuations, and the irrelevance to velocity sign and magnitude, are properties of the LDV approach, making it superior to the hot-wire one. Calibration of the LDV is not necessary, which considerably simplifies the measurement process. Since temperature inside the tunnel reaches 200°C, solid thermally resistant particles are seeded into the flow. To generate the particles, a 5% water solution of Na_2SO_4 is used. It is dispersed by a jet atomizer to produce an aerosol of saltwater droplets of approximately 2 μm. After quick evaporation of the water, the remaining salt crystals have an average size of approximately 0.8 μm. Particles of such size follow the flow very well. On account of the high refraction index, they deliver intensive scattered light signals. Compared with other salt materials, Na_2SO_4 has the advantage of being neither toxic nor corrosive.

For temperature measurements, the resistance-wire technique is employed. A platinum-plated tungsten wire of 1.25-mm length and 2.5-μm diameter is used. Temperature is determined by measuring the electric resistance of the wire, which is dependent on the ambient temperature. The resistance-wire technique provides good spatial and temporal resolution of temperature measurements in the tunnel.

When measuring temperature and velocity simultaneously, the velocity control volume and the temperature probe are placed at the same height, with the temperature probe shifted by 1 mm downstream, so as not to disturb the velocity field.

A laser light sheet technique is applied to qualitatively evaluate two-dimensional flow patterns along the longitudinal axis of the tunnel. The light sheet illuminates a thin layer of the flow in which a fog tracer is inserted. This layer can be portrayed with a digital television camera. By means of digital image processing, contrast and brightness of the visualized pattern may be improved. To generate the light sheet, a laser beam is spread in a vertical plane by a biconvex spherical lens and a convex cylindrical lens. The divergence angle of the light sheet is set at 17°; its thickness is approximately 5 mm. From the visualized flow pattern, typical sizes of the rising thermals, their heights, and frequencies can be estimated.

c. Evaluation of the tunnel for simulating the atmospheric CBL

The operating ranges of the tunnel with respect to different parameters of the flow were investigated while evaluating the tunnel for modeling atmospheric convection. The objectives of these investi-

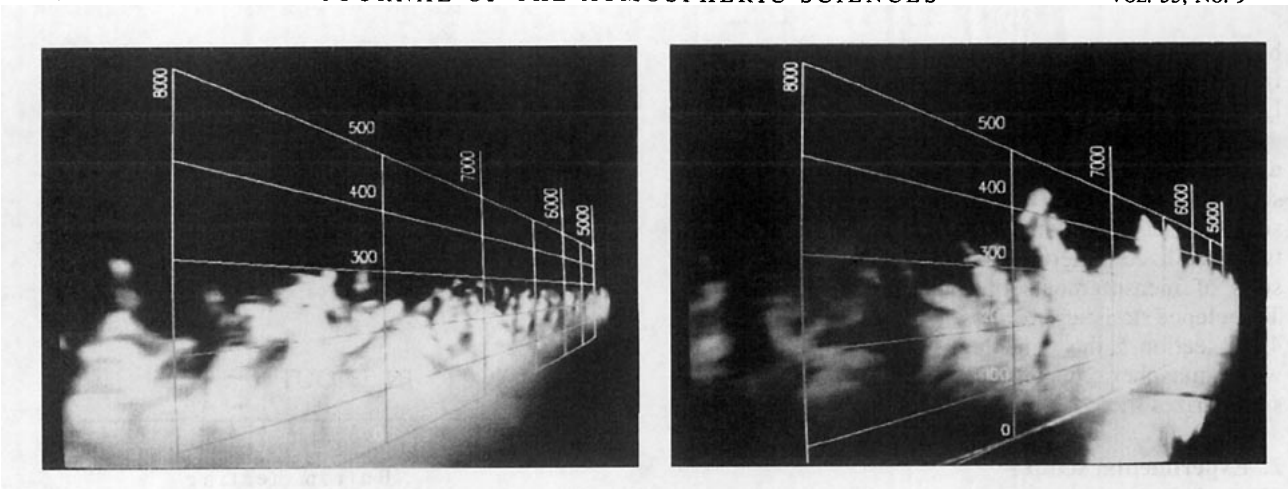

FIG. 2. (a) Visualized patterns of the turbulent flow in the tunnel without heating from the bottom and (b) with the heat flux of 1250 W m^{-2} through the floor of the test section. Conditions of the incoming flow: ΔT = 30 K at z = 0.3 m; u = 1 m s^{-1} is uniform with height. Dimensions of the imposed grid are given in millimeters.

gations were to obtain stable flow conditions and to meet the similarity requirements for simulating the atmospheric CBL.

At present, the tunnel can only be heated. This imposes certain restrictions on the experimental ranges of the temperature increment at the mixed-layer upper interface, the temperature gradient above it, and the bottom heat flux. Their maximum operating values were found to be 40 K, 67 K m^{-1} (10 K $layer^{-1}$), and 1500 W m^{-2}, respectively. For the approaching flow velocity, a lower limit of 0.5 m s^{-1} was established empirically. To avoid the effect of the ceiling, the maximum depth of the developed CBL is restricted to 0.6 m, which is 40% of the height of the test section.

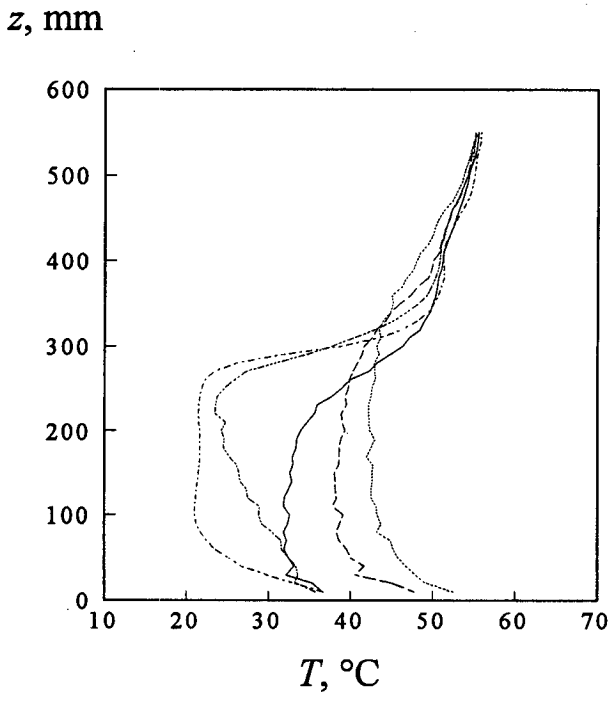

FIG. 3. Evolution of the mean temperature field along the longitudinal axis of the wind tunnel. Temperature profiles are measured at x = 0.68 m (dashed–dotted line), x = 2.33 m (dashed–double-dotted line), x = 3.98 m (solid line), x = 5.63 m (dashed line), and x = 7.28 m (dotted line).

In Fig. 2 two visualized wind flow patterns are presented. The first one represents a case without surface heating, with a temperature jump of ΔT = 30 K at z = 0.3 m in the approaching flow. The second pattern is obtained with the same initial temperature profile but with a heat flux of 1250 W m^{-2} from below. The flow direction in the plots is from right to left, and the fog is colored white. The neutral boundary-layer flow (Fig. 2a) is characterized by small-scale turbulence and negligible vertical exchange across the capping inversion. In contrast, large turbulent structures (thermals) are observed in the buoyancy-driven convective layer (Fig. 2b). They cause intensive mixing in the lower flow region and deeply penetrate into stably stratified upper layers. The effect of entrainment of the fresh air from above the inversion down into the mixed layer can also be seen in the second pattern. Penetrative thermals have tower or plumelike shapes. Their diameters decrease with height, as was also observed by Hooper and Eloranta (1986) in the atmospheric CBL. The maximum height of the thermals in the simulated CBL is about 550 mm. According to the definition of Nelson et al. (1989), this height can be taken as the upper boundary of the entrainment zone. A typical horizontal scale of rising thermals (updrafts) is approximately 200 mm. The downdrafts have a typical horizontal extension of about 600 mm. Quantitatively, the proportion between the horizontal scales of updrafts and downdrafts in the wind tunnel CBL corresponds fairly well with the atmospheric estimates by Lenschow and Stephens (1980). The qualitative similarity of the buoyant struc-

tures in the wind tunnel and the atmospheric prototypes visualized by lidar (Stull 1988) is even more striking.

An example of the development of the vertical temperature profile along the test section is shown in Fig. 3. The temperature increment in the approaching flow is 30 K, and the temperature gradient in the upper region is 33 K m^{-1}. A transition region, characterized by the penetration of convective turbulence into the initially neutrally stratified and slightly turbulent lower layer, occupies roughly the first 3 m of the test section. The shape of the temperature profile changes abruptly between $x = 2.33$ and $x = 3.98$ m. Within this range the vertical distribution of temperature gains the typical CBL form: a steep decrease of temperature in the near-surface layer, an approximate thermal uniformity within the mixed layer, marked temperature gradients in the interfacial layer, and a quiescence of temperature field in the turbulence-free stably stratified region, where remains of the initially generated layered structure can be observed. Downstream from $x = 3.98$ m, the CBL depth, which can be roughly estimated from the elevation of the capping inversion midpoint, increases progressively with distance. This growth is accompanied by cooling of the stably stratified layer due to the entrainment of warmer air from above the inversion into the bulk of the mixed layer. At $x = 3.98$ m and subsequent locations, the kinematic heat flux profiles (see Figs. 4b and 5a) are also characteristic of the developed CBL, in which the turbulence and the mean flow are in quasi-equilibrium.

Now, we consider the list of key parameters for simulating the atmospheric CBL in the thermally stratified wind tunnel. The two following dimensionless combinations are commonly used to characterize a CBL developing on the background of stable stratification (e.g., Deardorff et al. 1980; Zilitinkevich 1991; Fedorovich and Mironov 1994). The Richardson number based on the temperature increment ΔT across the interfacial layer:

$$\mathrm{Ri}_{\Delta T} = \beta w_*^{-2} z_i \Delta T,$$

and the Richardson number based on the buoyancy frequency N in the turbulence-free zone:

$$\mathrm{Ri}_N = N^2 z_i^2 w_*^{-2}.$$

It follows from the analysis by Meroney and Melbourne (1992) and Rau and Plate (1994) that the CBL with the surface shear Richardson numbers $\mathrm{Ri}_{\Delta T}$ and Ri_N have to be supplemented with the ratio u_*/w_* (or U_c/w_*) characterizing the proportion of the shear and buoyant contributions to turbulence production. One more important dimensionless parameter is the Reynolds number: $\mathrm{Re} = U_c L_c/\nu$. In the above combinations, $\beta = g/T_0$ is the buoyancy parameter, g is the acceleration due to the gravity, and T_0 is the reference temperature; $w_* = (\beta Q_s z_i)^{1/3}$ is the Deardorff convective velocity scale; Q_s is the near-surface value of $Q = \overline{w'T'}$, the turbulent kinematic heat flux; z_i is the inversion height usually defined as the level of the most negative heat flux of entrainment within the interfacial layer; $u_* = \tau_s^{1/2}$ is the friction velocity, τ_s is the near-surface value of $\tau = -\overline{w'u'}$, the turbulent shear stress normalized by density; U_c and L_c are the characteristic velocity and length scales of the flow, respectively; and ν is the kinematic viscosity of the air.

Under typical convective conditions in the atmospheric boundary layer, $\mathrm{Ri}_{\Delta T}$ and Ri_N are within the range of 0–100, and Re varies in the interval from 10^6–10^{10}, provided the mean-flow velocity and inversion height are taken as characteristic velocity and length scales. In the wind tunnel $\mathrm{Ri}_{\Delta T}$ up to 10 and Ri_N up to 20 can be achieved at present, which in the atmosphere corresponds to comparatively weak stratifications across the inversion layer and above it. The equality of the Re numbers in the atmosphere and in the tunnel cannot be ensured. The characteristic values of Re in the present experiments were of the order 10^5. Such Re are large enough to presume that molecular diffusivities are unimportant in the main part of the simulated CBL, and hence the reproduced turbulent regime can be taken as Re independent.

Turbulence production in the atmospheric boundary layer is assumed to be dominated by convection when the ratio u_*/w_* is sufficiently small. It is easy to express u_*/w_* through another ratio characterizing the CBL turbulence close to the surface, namely $-L/z_i$, where $L = -u_*^3/(\beta k Q_s)$ is the Monin–Obukhov length scale and k is the von Kármán constant. Using the definition of the convective velocity scale, we have $u_*/w_* = -(kL/z_i)^{1/3}$. Following Holtslag and Nieuwstadt (1986), the shear contribution to the turbulence production in the CBL can be neglected if $-L/z_i < 0.1$, which gives $u_*/w_* = 0.34$ as a conventional boundary value to distinguish between the regimes of shear and shear-free convection. For most of cases studied in the tunnel, u_* was from 0.03 to 0.08 m s^{-1} and w_* was from 0.15 to 0.20 m s^{-1}, and thus the values of u_*/w_* were within the range of 0.2–0.5. This yields $0.02 < -L/z_i < 0.3$, which is around the margin for the shear effects. The influence of the surface shear on turbulence statistics will be discussed below.

The effect of the earth's rotation on the turbulence regime in the atmospheric CBL is left beyond our studies. Under the conditions of buoyancy-driven turbulent mixing in the lower atmosphere, this effect is negligible if the characteristic eddy turnover timescale is small compared with $1/f$, where f is the Coriolis parameter. This holds in the atmospheric CBL for most of the turbulent motions except, perhaps, for large-scale helical circulations, which may be affected by the rotation.

Based on results of the test experiments and similarity considerations, the following setup was chosen for the present study: the two lower layers of the tunnel, of 0.3-m depth in total, operate in the open-circuit regime, with the incoming flow possessing the temperature of the ambient atmospheric air; between the sec-

ond and the third layers, a temperature jump of 30 K is imposed; the temperature of each of the subsequent layers is controlled to produce a temperature gradient of 33 K m^{-1} (5 K $layer^{-1}$) in the upper flow region; and the incoming flow velocity in all layers is set equal to 1 m s^{-1}. With the uniform heat flux through the bottom of up to 1250 W m^{-2}, this configuration was found to be steady and sufficient to simulate a quasi-stationary, horizontally evolving CBL.

A convective layer of similar type can be observed in the atmosphere when the advection of neutrally stratified air over a heated surface takes place, for example, during the transformation of a seaborne air mass over a heated near-shore terrain. Because conditions are steady, we use the ergodic theorem and calculate turbulence statistics, applying time averaging. In experiments with nonsteady CBL, the statistics are commonly obtained by area averaging.

The Taylor hypothesis can be invoked in our case as a background for relating temporal and spatial scales of turbulent motions in the simulated CBL. The wind tunnel profiles of mean velocity and turbulence variances of velocity components, discussed in the next section, bear witness that the Taylor hypothesis is satisfied fairly well in the wind tunnel flow, since the turbulence intensity is small compared to the mean-flow velocity (Willis and Deardorff 1976).

3. Characteristics of the mean flow

Profiles of mean temperature, and horizontal and vertical velocity components—measured at three locations within the test section of the tunnel—together with the turbulent kinematic heat flux for the same locations are presented in Fig. 4. All profiles to be considered in sections 3 and 4 refer to the fetches ≥3.98 m, thus, representing a fully developed CBL.

In the present study the mean temperature and the heat flux values have been measured independently like in Deardorff and Willis (1985). In the earlier water tank experiments of Deardorff et al. (1969) and Deardorff et al. (1980), $Q = \overline{w'T'}$ was derived from the evolution of the mean temperature field.

From the profile of the turbulent kinematic heat flux, the inversion height z_i can be defined as the elevation of the heat-flux minimum in the upper part of the CBL. Using this traditional definition, it is possible to trace a progressive growth of the CBL depth in the plots of $Q = \overline{w'T'}$ (Fig. 4b) and in relevant temperature graphs (Fig. 4a). The positions of the heat flux minima roughly correspond to the centers of the temperature inversion layers, which is a CBL feature well known from atmospheric measurements (Caughey and Palmer 1979), water tank studies (Willis and Deardorff 1974; Deardorff et al. 1980; Deardorff and Willis 1985), and LES (Moeng 1984; Mason 1989; Schmidt and Schumann 1989).

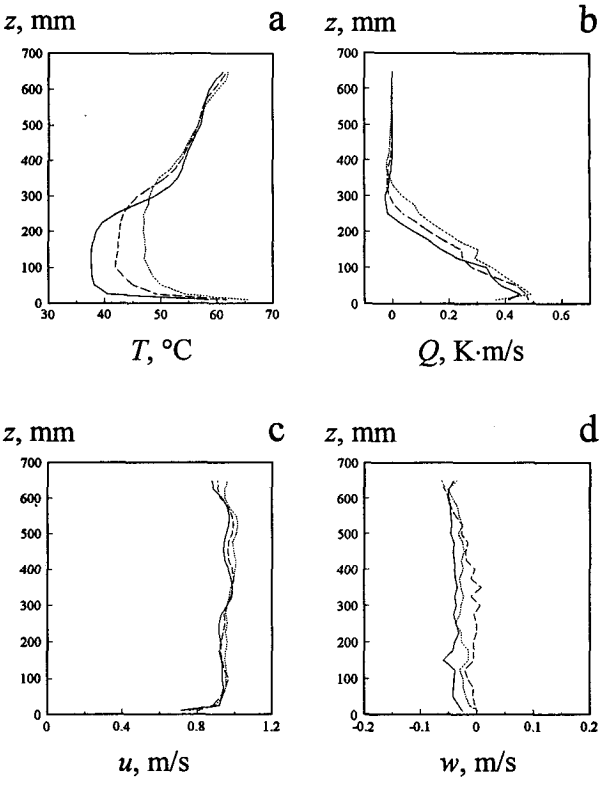

FIG. 4. Profiles of (a) the mean-flow temperature, (b) turbulent kinematic heat flux, and (c) longitudinal and (d) vertical components of the mean-flow velocity in the simulated convective boundary layer at x = 3.98 m (solid line), x = 5.63 m (dashed line), and x = 7.28 m (dotted line).

As seen from the patterns of longitudinal velocity components in Fig. 4c, the approximate uniformity of the velocity field with height is retained at all stages of the CBL development. The velocity shear is confined to the shallow near-surface layer. Slight velocity shears can also be noticed at the levels roughly corresponding to inversion heights. These elevated shear regions shift upward as the CBL grows. Vertical profiles of velocity within the mixed layer are quite similar to the temperature profiles shown in Figs. 4a but have opposite curvature. The main source of heat is located at the bottom and, thus, it is transported upward. On the contrary, the momentum, which has a sink at the underlying surface, is transported downward. This causes profiles of temperature and velocity in the main portion of the CBL to be qualitatively mirror images of each other.

Profiles of the mean-flow vertical velocity at three longitudinal locations are shown in Fig. 4d. The values of w at all measurement levels are close to zero, with a slight tendency to be negative. No marked systematic correlations between longitudinal changes of the horizontal velocity and variations of the vertical velocity can be revealed from the u and w plots in Fig. 4.

It is likely that the observed mean vertical motions in the simulated CBL are associated with quasi-steady transverse helical circulations, which are quite common for the CBL with shear and somewhat similar to horizontal roll vortices observed in the atmospheric CBL (Stull 1988). These larger-scale motions enhance the mixing in the CBL, interact with convective turbulence, and thus contribute to the exchange between the mixed layer and stably stratified air aloft. As preliminary velocity measurements in the y–z planes have shown, the characteristic magnitude of w in the test section is about 0.04 m s^{-1}, being much smaller than the mean-square values of the vertical velocity fluctuations, which are typically about 0.15 m s^{-1}. Average values of w at the fixed elevations in the cross section are close to zero. The magnitude of the local mean-flow transverse velocity (y component) was found to be of the order of w.

4. Turbulence statistics

We show the profiles of turbulence statistics from the wind tunnel measurements made dimensionless using the traditional Deardorff (1970) convective scales: z_i for the height, $w_* = (\beta Q_s z_i)^{1/3}$ for the velocity, and $T_* = Q_s/w_*$ for the temperature. Most CBL turbulence measurements and model simulations, presented in the literature, employ these scales. Ranges of their validity and the extent to which the resulting dimensionless profiles can be considered as universal were widely discussed in numerous articles devoted to the subject, for instance, in the review by Wyngaard (1992). Despite shortcomings, the Deardorff mixed-layer scaling continues to be a convenient tool for comparison of measurements from different experiments and for verification of simulation results.

In the wind tunnel experiment the convective scales are determined from the measured profiles of the turbulent kinematic heat flux $Q = \overline{w'T'}$. Close to the surface, the direct evaluation of Q_s from the correlation between w' and T' is not representative because molecular heat transfer plays an important part in this region. In particular, we suppose that the near-floor irregularities in some Q profiles presented in Fig. 4b appear because the turbulence at small heights is not fully developed. The second limitation is a technical one and associated with the size ratio of the temperature probe and the control volume of velocity measurements. The third factor is relevant to sharp variations with height of both vertical velocity and temperature fluctuations near the surface. These variations are such that a small vertical shift between measuring points of velocity and temperature can induce substantial errors of the Q calculation. An alternate method of estimating Q_s, which is from the output of the bottom heating system, is not accurate enough due to uncertainty in evaluating the heat transport by the semiorganized motions and small but unavoidable heat losses through the walls of the test section. Based on the above considerations, the value of Q_s has been estimated at every measurement location by a linear extrapolation of the Q profile to $z = 0$. The normalized profiles of the turbulent kinematic heat flux are presented in Fig. 5a.

Vertical distributions of the turbulent momentum flux depicted in Fig. 5b are not as smooth as profiles of heat flux determined at the same locations. This may be a result of the local quasi-steady circulations mentioned in the previous section. Changes of turbulent shear profile with distance indicate that shear effects play more important part at small fetches, during the early stages of CBL evolution. Hence, one may expect the variances of the velocity components, which constitute turbulence kinetic energy (TKE), to be more affected by the shear at $x = 3.98$ m rather than at subsequent locations. Within the mixed core of the developed CBL, the magnitude of the momentum flux decreases with height. The level of $\overline{w'u'}$ vanishing roughly corresponds to the height of the heat flux degeneration in Fig. 5a.

The contributions of shear and buoyancy to the TKE budget in the horizontally evolving CBL can be approximately evaluated using a simple two-dimensional

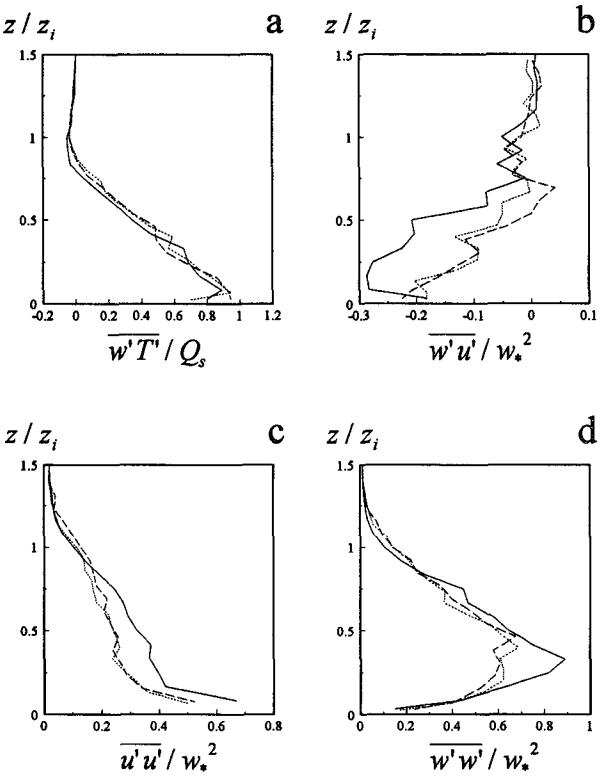

FIG. 5. (a) Normalized profiles of the turbulent kinematic heat flux, (b) turbulent flux of momentum, and (c) variances of horizontal and (d) vertical velocity components in the simulated convective boundary layer at $x = 3.98$ m (solid line), $x = 5.63$ m (dashed line), and $x = 7.28$ m (dotted line).

zero-order jump model for the convective flow in the tunnel. Test measurements over the cross sections of the tunnel indicate that transverse variations of the flow in the simulated CBL are small, and thus they may be neglected. For the nonsteady CBL zero-order jump, bulk models have been exploited widely since the 1960s, when they were introduced by Ball (1960) and Lilly (1968).

Departing from the Reynolds equations of momentum and heat balance and employing zero-order jump parameterizations of the velocity and temperature profiles over the CBL, the momentum and heat budgets in the quasi-stationary horizontally evolving CBL can be obtained (for the derivation see the appendix):

$$z_i\bar{\bar{u}}\frac{d\bar{\bar{u}}}{dx} = \Delta u\frac{d\bar{\bar{u}}\bar{z}_i}{dx} + \frac{\beta}{2}\frac{dz_i^2\bar{\bar{T}}}{dx} - \tau_s, \quad (1)$$

$$z_i\bar{\bar{u}}\frac{d\bar{\bar{T}}}{dx} = \Delta T\frac{d\bar{\bar{u}}\bar{z}_i}{dx} + Q_s, \quad (2)$$

where $\bar{\bar{u}}$ is the average mixed-layer value of the longitudinal component of the mean flow velocity, $\Delta u = u_{z_i} - \bar{\bar{u}}$ is the increment of this component across the mixed-layer upper interface, and u_{z_i} is the value of u in the stable layer at the upper side of the CBL interface represented by the surface of zero-order discontinuity at $z = z_i$. Analogous notation is used for temperature. The operation of averaging is defined as $(\bar{\bar{}}) = (1/z_i)\int_0^{z_i}(\ )dz$.

In the simulated CBL the advection term [left-hand part of (1)], the acceleration term relevant to the CBL heating, and the turbulent friction term are within the range from 10^{-3} to 10^{-2} m^2 s^{-2}. They are the main components of the momentum budget (1), while the entrainment term incorporating velocity jump is at least one order of magnitude smaller as shown in the velocity and temperature profiles in Figs. 4a and 4c. In the heat budget equation (2), all three terms are of the same order (advection of heat, which is about 1 K m s^{-1}, is balanced by the entrainment and surface heating, both of 0.5 K m s^{-1}.

The momentum and heat flux profiles, relevant to the zero-order jump parameterizations, are

$$\tau = \tau_s(1-\zeta) + \Delta u\frac{d\bar{\bar{u}}\bar{z}_i}{dx}\zeta + \frac{\beta}{2}z_i^2\frac{d\bar{\bar{T}}}{dx}\zeta(\zeta-1), \quad (3)$$

$$Q = Q_s(1-\zeta) - \Delta T\frac{d\bar{\bar{u}}\bar{z}_i}{dx}\zeta, \quad (4)$$

where $\zeta = z/z_i$ is the dimensionless height. Equations (3) and (4) follow from the momentum and heat balance equations in the Reynolds form integrated from 0 to $z < z_i$ using (1) and (2). The derivation is given in the appendix.

It is seen from (3) and (4) that within the framework of the zero-order jump approach both fluxes undergo zero-order discontinuities at the mixed-layer interface. From its lower side, at $z = z_{i-}$, they gain values $\Delta u(d\bar{\bar{u}}\bar{z}_i/dx)$ and $-\Delta T(d\bar{\bar{u}}\bar{z}_i/dx)$, respectively, being both equal 0 at $z \geq z_{i+}$. According to (4), the heat flux is linear, which conforms with the measured Q profiles in Fig. 4b. Departure from the linearity of the momentum flux profile is determined by the last term of (3), representing the contribution of the horizontal temperature changes. It is probable that this contribution is responsible for deformation of the turbulent stress distribution at $x = 3.98$ (Fig. 5b), where the mean temperature growth in the horizontal is substantial.

The expressions of the turbulent fluxes of momentum and heat can be substituted in the TKE balance equation. Its integration over the CBL depth (see appendix) gives the entrainment rate equation

$$\left[\bar{\bar{e}} - \frac{1}{2}(\Delta u^2 - \beta z_i\Delta T)\right]\frac{d\bar{\bar{u}}\bar{z}_i}{dx} + \left(\bar{\bar{u}}\frac{d\bar{\bar{e}}}{dx} - \frac{\beta}{2}Q_s + \bar{\bar{\epsilon}}\right)z_i = \bar{\bar{u}}\tau_s - \Phi_{z_i}, \quad (5)$$

which is the TKE budget in the CBL. In (5), Φ_{z_i} is the vertical transport of energy at the CBL top and $\bar{\bar{e}}$ and $\bar{\bar{\epsilon}}$ are the CBL averages of turbulence kinetic energy per unit mass, e, and its dissipation rate ϵ.

Because the velocity increment across the entrainment layer in the wind tunnel flow is small, and $\bar{\bar{u}}$ and z_i change only slightly with x, it is reasonable to expect that the top-down shear contribution [here we use terminology introduced by Wyngaard and Brost (1984)], represented in (5) by $-\frac{1}{2}\Delta u^2(d\bar{\bar{u}}\bar{z}_i/dx)$, does not substantially affect the TKE budget. On the other hand, the surface shear is likely to noticeably modify the turbulence regime. In our experiments, the product $\bar{\bar{u}}\tau_s$, representing the bottom-up shear effect, has a typical value of 2.5×10^{-3} m^3 s^{-3}, which is quite close to that of the bottom-up buoyancy contribution $(\beta/2)Q_sz_i \approx 3 \times 10^{-3}$ m^3 s^{-3}, the main production term of (5). The top-down buoyancy term $\frac{1}{2}\beta z_i\Delta T(d\bar{\bar{u}}\bar{z}_i/dx)$ is slightly smaller by the magnitude (2×10^{-3} m^3 s^{-3}) than any of the bottom-up ones, whose joint effect is dominant in the simulated CBL.

The expected enhancement of TKE at small fetches by shear turbulence is seen clearly from the profiles of u and w variances in Figs. 5c and 5d. Both horizontal and vertical velocity fluctuations measured at $x = 3.98$ m are affected by the shear. At larger fetches, the $\overline{u'u'}$ and $\overline{w'w'}$ profiles demonstrate more or less universal behavior when plotted in the dimensionless form using the Deardorff convective scales. Values of the horizontal velocity variance are largest near the surface due to local horizontal motions in the zones of convergence (divergence) at the feet of the thermals (downdrafts). An additional factor of the $\overline{u'u'}$ enhancement close to the surface is the contribution of the mean-flow

shear. Analysis of Stull (1988) gives reasons to assume that the horizontal velocity variance is more sensitive to the influence of the surface shear than $\overline{w'w'}$. Above the surface layer, the values of $\overline{u'u'}$ gradually decrease with height. In the vicinity of the inversion level, slight bends can be observed in the $\overline{u'u'}$ profiles. These irregularities, which appear as changes of slope, are caused by sideward spreading of the ascending air, transported by the thermals, under the capping inversion. We shall see later that $\overline{u'u'}$ acquires a local maximum at $z = z_i$ if the inversion is sufficiently strong.

The vertical velocity variances reach their maximum values of about 0.4 at z/z_i. Besides enhancement by the shear, the vertical velocity fluctuations are also affected by the local quasi-steady motions, which were discussed while presenting the measurements of the mean vertical velocity. These effects are more pronounced at smaller fetches, and larger values of w variance at $x = 3.98$ m in Fig. 5d may be explained, at least partially, by their contribution.

From the evolution of the $\overline{u'u'}$ and $\overline{w'w'}$ profiles over the test section the contribution of advection to the TKE budget of the simulated CBL can be estimated. By first evaluating e as $\overline{u'u'} + \frac{1}{2}\overline{w'w'}$ and then estimating the term of (5) responsible for integral changes of e due to advection, $d\overline{\bar{e}\bar{u}}z_i/dx = \bar{\bar{e}}(d\bar{u}z_i/dx) + \bar{\bar{u}}z_i(d\bar{\bar{e}}/dx)$, we find it to be at least one order of magnitude smaller than the main terms of (5), namely, the buoyancy and the surface-shear ones. To assess Φ_{z_i}, the energy drain by the gravity waves from the top of the simulated CBL, we may employ either one of the alternative parameterizations proposed by Kantha (1977)—$\Phi_{z_i} \propto \beta Q_s \Delta h^2 z_i^{-1}\ \mathrm{Ri}_N^{3/2}$—or Zilitinkevich (1991)—$\Phi_{z_i} \propto \beta Q_s \Delta h^3 z_i^{-2}\ \mathrm{Ri}_N^{3/2}$—both based on the Thorpe (1973) wave generation theory. In these expressions, Δh is the entrainment layer depth. Fedorovich and Mironov (1994) found that coefficients of proportionality in the above parametric formulas are of the order of 10^{-2} and less. For typical conditions in the simulated CBL ($\beta = 0.025$, $Q_s = 0.5$ K m s^{-1}, $\Delta h = 0.15$ m, $z_i = 0.4$ m, $\mathrm{Ri}_N = 10$), we obtain from the first parameterization $\Phi_{z_i} < 3 \times 10^{-4}$ m^3 s^{-3} and from the second one $\Phi_{z_i} < 10^{-4}$ m^3 s^{-3}. Thus, we infer that the TKE balance is not significantly affected by the wave-related energy drain in our case.

Normalized profiles of the temperature variances in Fig. 6a are characterized by a sharp drop of $\overline{T'T'}$ with height in the near-surface region, where the mean temperature also decreases sharply with z, see Fig. 4a. In the lower part of the mixed layer the normalized profiles of the temperature variance are similar at all longitudinal positions. At the CBL top, where the temperature fluctuations are enhanced by the temperature difference across the interfacial layer, the dissimilarities between the profiles become distinctive. A marked correlation between the $\overline{T'T'}$ maximum, located approximately at the inversion level, and the stable lapse

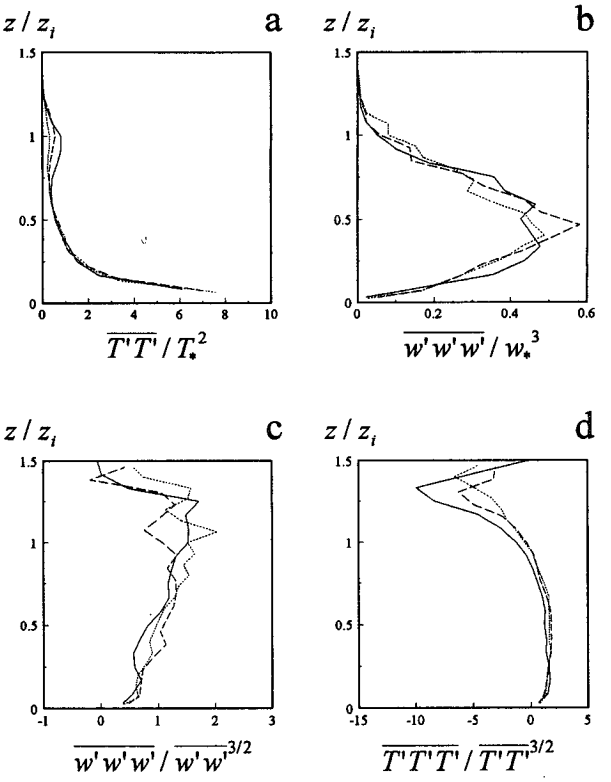

FIG. 6. (a) Normalized profiles of the temperature variance, (b) the triple moment of the vertical velocity fluctuations, and (c) the skewness of the vertical velocity and (d) temperature fluctuations in the simulated convective boundary layer at $x = 3.98$ m (solid line), $x = 5.63$ m (dashed line), and $x = 7.28$ m (dotted line).

rate across the inversion is revealed by comparison of the mean and variance temperature profiles in Figs. 4a and 6a.

The vertical turbulent transport of TKE represented in Fig. 6b by the vertical distributions of $\overline{w'w'w'}$ reaches its maximum roughly in the middle of the CBL. Over most of the layer, the transport is positive and therefore directed upward. Measured profiles of $\overline{w'w'w'}$ attest that inside the mixed layer upward motions with positive values of w' occupy shorter time intervals and, thus, are narrower but have larger absolute values than motions with negative w' relevant to downdrafts. Above the mixed layer the values of $\overline{w'w'w'}$ tend to zero, being slightly negative in the upper portion of the interfacial layer.

The last statistics to be discussed in this section are the skewnesses of the vertical velocity and temperature fluctuations. They are shown in Figs. 6c and 6d. As a statistical quantity, the skewness characterizes the asymmetry of the distribution of a random value and the proportion between the ranges of its positive and negative fluctuations. The skewness of w in the bulk of the mixed layer (Fig. 6c) is positive and grows with height. This indicates that the range of positive vertical

velocity values increases toward the interfacial layer. The vertical velocity skewness reaches the maximum at the inversion level, in the vicinity of $z/z_i = 1$. As seen from the profiles of the temperature skewness in Fig. 6d, the proportion of positive and negative temperature fluctuations at this level is not the same. The air in the thermals cools down in the process of ascending, and at the foot of the interfacial layer the temperature skewness, which was positive in the mixed layer, becomes zero, indicating that positive and negative temperature fluctuations at this level are statistically equivalent. At larger heights the temperature skewness is negative. Temperature fluctuations variance within this range of heights is very small, see Fig. 6a, so the distribution of temperature fluctuations is extremely narrow and with long negative tail, which is the effect of sparse and comparatively cool thermals reaching the edge of the interfacial layer. We think that this is a feature of the reproduced convective regime characterized by deep penetration of thermals into stably stratified outer flow with some slight entrainment of the warm air downward.

5. Comparison with atmospheric, water tank, and LES data

We compare results of the wind tunnel simulations with the data of atmospheric measurements collected during field experiments in Minnesota and Ashchurch (Caughey and Palmer 1979), the Air Mass Transformation Experiment (Lenschow et al. 1980), and experiments in Limagne and Beauce, France, data of which are given in Sorbjan (1991). Results of water tank simulations by Deardorff and Willis (1985) and LES data of Schmidt and Schumann (1989) are also attracted for comparison.

The atmospheric data employed represent well-developed convection, for which $-L/z_i \ll 1$. The particular values of Richardson numbers $\mathrm{Ri}_{\Delta T}$ and Ri_N in the atmospheric CBL are not presented in the quoted papers. Profiles of turbulence statistics are quite sensitive to both quantities, and the Richardson number differences can be a source of data scatter when results from different experiments are plotted together. In the water tank study of the shear-free CBL by Deardorff and Willis (1985), according to their own estimate, the characteristic value of $\mathrm{Ri}_{\Delta T}$ was about 15, and Ri_N was reaching 150. These reevaluated numbers are about one order of magnitude smaller than our previous estimates given in Fedorovich et al. (1995). Large eddy simulations of shear-free convection by Schmidt and Schumann (1989), which we use for comparison of the data referring to dimensionless time $t_* = 6.5$, were performed at $\mathrm{Ri}_{\Delta T} = 25$ and $\mathrm{Ri}_N = 100$. The typical values of $\mathrm{Ri}_{\Delta T}$ and Ri_N in our wind tunnel experiments were 5 and 10, respectively.

From the results shown in Figs. 5 and 6 we employ for comparison those that correspond to well-developed convection with marked entrainment at the CBL top, established profiles of mean-flow characteristics, and moderate contribution of the shear effects to the turbulence production ($u_*/w_* \approx 0.3$). Thus, we consider exclusively hereafter statistics derived from the measurements at $x > 5$ m.

In Fig. 7a, Q profiles from the wind tunnel experiments are compared with atmospheric measurements, results of water tank modeling, and LES. Atmospheric points display a considerable scatter, and their vertical distribution within the mixed layer can hardly be approximated by a linear function. One may expect that this departure from linearity in the atmospheric profile of Q is due to contributions to the heat balance of the CBL other than the convective heating. Results of the wind tunnel experiments fit a linear law very well, being in good conformity with the data of LES and water tank measurements over the lower portion of CBL, up to $z/z_i = 0.8$. In the interfacial layer, the negative heat flux of entrainment from the wind tunnel measurements is much smaller compared to the minimum of Q observed in the atmospheric, water tank, or LES studies. This is due to the weaker inversion (characterized by the smaller $\mathrm{Ri}_{\Delta T}$) in the wind tunnel that reduces the magnitude of temperature fluctuations in the interfacial layer.

Wind tunnel values of the correlation coefficient between the vertical velocity and temperature fluctuations are in fair agreement with the predictions of LES and the results of the water tank experiments, see Fig. 7b. In the upper part of the CBL, where substantial discrepancies between the heat flux profiles are observed in Fig. 7a, this agreement finds its explanation in reduced σ_T within the entrainment zone as a result of moderate inversion strength in the wind tunnel experiments (see also Fig. 9a). Atmospheric measurements give smaller values of $r_{wT} = \overline{w'T'}/(\sigma_w \sigma_T)$ in the main portion of the mixed layer, which may be another manifestation of nonconvective heating in the atmospheric CBL.

The scatter between data from the different sources in Fig. 8a, presenting the normalized profiles of the horizontal velocity variance, is rather large. Schmidt and Schumann (1989) argue that their LES model correctly predicts the horizontal velocity variance for a dry CBL with zero mean speed, while the water tank simulations of Deardorff and Willis (1985) and the atmospheric measurements of Caughey and Palmer (1979), both giving higher values of $\overline{u'u'}$, were affected by horizontal variations of the surface heat flux in the first case and by the presence of the surface shear in the second. All three datasets are compared with the data of the wind tunnel experiments in Fig. 8a. We think that the argumentation of Schmidt and Schumann (1989) concerning the effects of shear is acceptable for the lower part of the CBL, where the wind tunnel simulations also predict higher values of the horizontal ve-

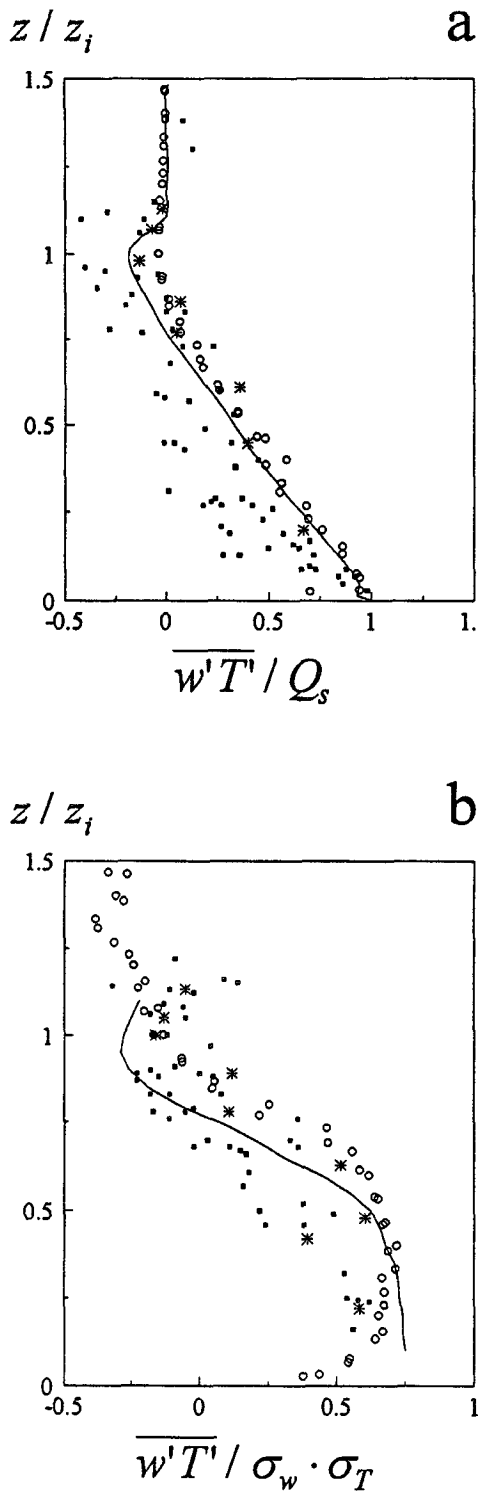

FIG. 7. Comparison of wind tunnel data (circles) on (a) vertical kinematic heat flux and (b) correlation coefficient between vertical velocity and temperature fluctuations with the results of (a) atmospheric measurements (filled squares) from Caughey and Palmer (1979) and (b) from Sorbjan (1991). The water tank simulations of Deardorff and Willis (1985), asterisks; and LES results of Schmidt and Schumann (1989), line.

locity variance apparently resulting from the surface shear. In the bulk of the mixed layer, the wind tunnel data are somewhere between the atmospheric and LES results. Near the CBL top, within the entrainment region, the intensity of the longitudinal velocity fluctuations is determined by two main mechanisms: a sideward transport of the air from the thermals under the inversion, and the enhancement of turbulence by the velocity shear across the interfacial layer. The latter effect, which was excluded in the LES and water tank studies, is likely to be one of the reasons for the large variances of u in the upper part of the atmospheric CBL. Destruction of rising thermals by the comparatively strong capping inversions, reproduced in the LES and water tank experiments, results in horizontal motions yielding marked maxima in the profiles of $\overline{u'u'}$ from these studies. A similar maximum, although not so pronounced, can be noticed in the distribution of the atmospheric data. Our experimental results, obtained with moderate $\mathrm{Ri}_{\Delta T}$ numbers, merely give some sort of a slope change (bend) in the horizontal velocity variance profile at z/z_i close to 1. From this, one may infer that the magnitude of the $\overline{u'u'}$ local maximum in the upper portion of CBL depends essentially on the inversion strength. Above the inversion, the decay of the horizontal velocity variance with height is faster, with larger values of Ri_N (LES and water tank data) characterizing the damping effect of buoyancy force in the outer flow region. Our data do not support the idea of Schmidt and Schumann (1989) concerning the increase of horizontal and vertical velocity variance with a decrease of the Froude number $\mathrm{Fr}_C = w_*/(Nz_i)$, which corresponds to the increase of Ri_N. In the wind tunnel experiments the characteristic values of Fr_C were 0.3 and more [compared to 0.1 in LES of Schmidt and Schumann (1989)], but velocity variances obtained were generally larger than the LES ones (see also Fig. 8b). This may be one more effect of the surface shear.

The discrepancies between the data of different origin on the vertical distribution of $\overline{w'w'}$ given in Fig. 8b are not as striking as those between the normalized profiles of $\overline{u'u'}$ in the previous plot. Within the main portion of the CBL, the data from the water tank and atmospheric measurements, as well as the LES results, are in good agreement with each other. The variances obtained from the wind tunnel simulations are slightly exaggerated compared with all other data, especially at $z/z_i < 0.5$. We explain this primarily by the effect of weak local circulations discussed in section 4. A certain role in the enhancement of $\overline{w'w'}$ at small z/z_i can also be attributed to the surface shear. Similarly to the vertical distributions of $\overline{u'u'}$, the decrease of $\overline{w'w'}$ with height at $z/z_i > 1$ displays dependence on strength of the stratification above the inversion layer, with larger Ri_N (e.g., in LES experiments) this decrease is steeper.

The most vivid distinctions between the convective regimes, characterized by different intensities of entrainment and by different Richardson numbers $\mathrm{Ri}_{\Delta T}$

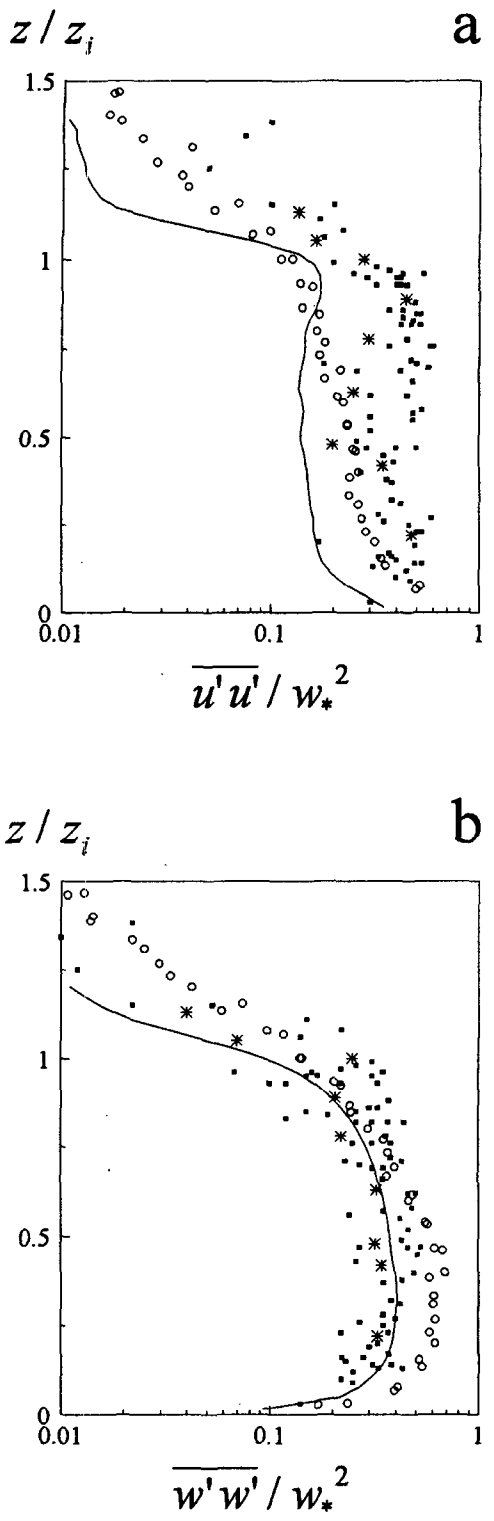

FIG. 8. Profiles of (a) horizontal and (b) vertical velocity variances in the simulated convective boundary layer (circles) as related to the atmospheric data of Caughey and Palmer (1979) and Lenschow et al. (1980): filled squares; water tank results of Deardorff and Willis (1985): asterisks; and LES data of Schmidt and Schumann (1989): solid line.

and Ri_N, are found in the normalized profiles of temperature fluctuations. This was noted by a number of authors while discussing the applicability of the Deardorff (1970) convective scales to turbulence variances in the CBL (e.g., Wyngaard 1992) or proposing, like Sorbjan (1990, 1991), new similarity scales for the CBL. Comparison of the wind tunnel data on $\overline{T'T'}$ vertical distributions with relevant profiles from the atmospheric, water tank, and LES experiments clearly demonstrates this effect (Fig. 9a). In the lower half of the CBL, where the turbulence structure of the layer is determined mainly by bottom-up effects, all considered datasets provide similar values of $\overline{T'T'}$. The discrepancies drastically increase near the top of the CBL. The temperature variances from the wind tunnel experiments are the smallest at $z/z_i = 1$, while water tank and large eddy simulations with stronger stabilities in the entrainment zone and above it (larger $Ri_{\Delta T}$ and Ri_N numbers) give values roughly 10 times higher than the temperature variance at the same dimensionless height. In the low-Re direct numerical simulation (DNS) of the sheared CBL by Coleman et al. (1994), with $Ri_{\Delta T} = 15$ and $Ri_N = 75$, the temperature variance in the inversion was found to be comparable with the Deardorff and Willis (1985) water tank results, although the DNS $\overline{u'u'}$ values at the CBL top were much smaller than those from the water tank study. Such underestimation of the horizontal velocity variance by the DNS could be characteristic of the simulated convection at low Re numbers.

Atmospheric measurements and LES give huge temperature variances above the CBL. In this region the $\overline{T'T'}$ values show inverse dependence on Ri_N compared with velocity variances: larger Ri_N numbers correspond to bigger temperature variances. Schmidt and Schumann (1989) explain considerable temperature fluctuations above the inversion by the effect of wavy motions, which become increasingly important with larger Ri_N. In the atmosphere an overestimation of $\overline{T'T'}$ may also be due to vertical displacements of an aircraft while measuring temperature fluctuations within the layers with large stable lapse rates.

Figure 9b presents results of the wind tunnel measurements of the third moment of the vertical velocity fluctuations compared with the data on $\overline{w'w'w'}$ from other experimental and model studies. As in the case of the second moment of w fluctuations, see Fig. 8b, wind tunnel values are the largest of all the data presented for the main part of the mixed layer. This is partially caused by the near-surface shear, but we also suspect $\overline{w'w'w'}$ to be enhanced by the flow instabilities resulting from the quasi-steady local circulations. Larger values of $\overline{w'w'w'}$ in the simulated CBL show that the disproportion between updrafts and downdrafts with respect to their size (extent in time) and strength is greater in the wind tunnel flow than in the atmosphere, water tank, and LES. Compact and fast-rising

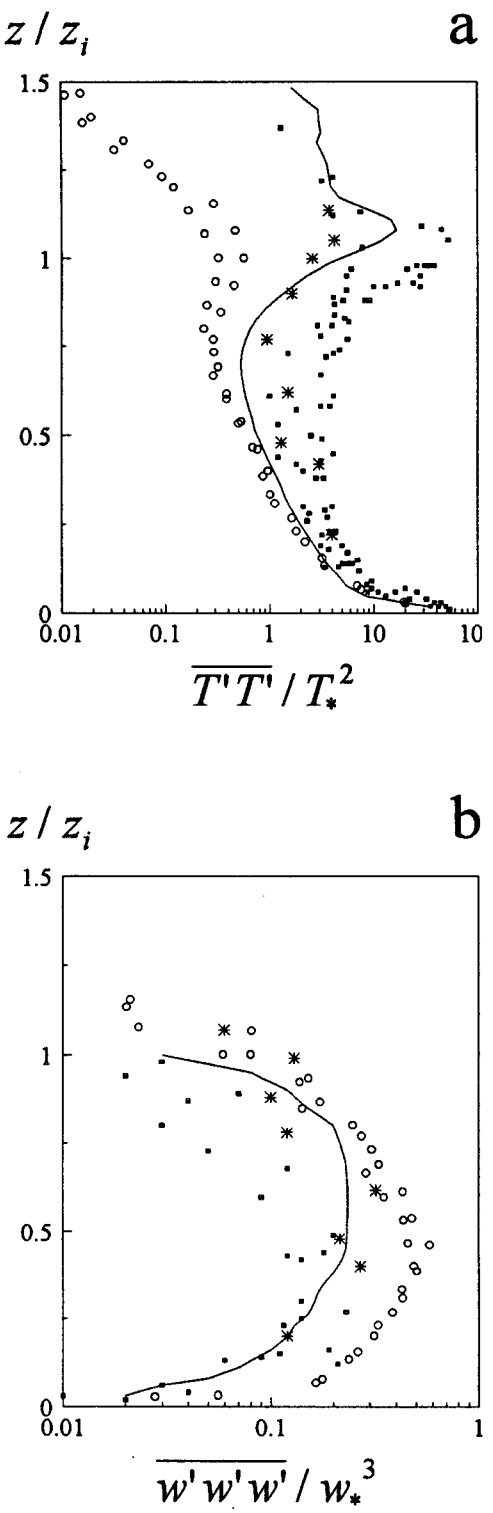

FIG. 9. Vertical distribution of (a) the dimensionless temperature variance and (b) the third moment of the vertical velocity fluctuations from the wind tunnel simulations (circles); atmospheric measurements (filled squares) of (a) Caughey and Palmer (1979) and (b) Lenschow et al. (1980); water tank experiments of Deardorff and Willis (1985): asterisks; and LES of Schmidt and Schumann (1989): line.

plumes of hot air are slightly affected by the organized motions, whose influence on the more extended and slower downdrafts can be substantial. This is perhaps the reason why the exaggeration of the vertical velocity fluctuations is larger in the range of heights $0.1 < z/z_i < 0.6$ (this is also true for the second moments of w fluctuations in Fig. 8b), where downdrafts considerably contribute to the vertical velocity variability.

Finally, we consider vertical distributions of the vertical velocity and temperature fluctuations skewness. Data on $\overline{w'w'w'}/(\overline{w'w'})^{3/2}$ are shown in Fig. 10a. For the temperature skewness we did not find data published from water tank studies or LES. Therefore, in Fig. 10b the wind tunnel data are compared only with atmospheric measurements. For the skewness of both w and T fluctuations, the wind tunnel results are in reasonable agreement with the data from the other sources. All datasets give positive values of the vertical velocity skewness in the bulk of the CBL, bearing witness to a wider range of values occupied by updrafts associated with positive fluctuations of w, rather than by downdrafts. The skewness observed in the atmosphere is quite uniform in the vertical, contrary to profiles obtained in laboratory and with LES, which clearly indicate growth of $\overline{w'w'w'}/(\overline{w'w'})^{3/2}$ with height. This discrepancy is explained if we consider together profiles of the vertical velocity variance and the triple moment of w fluctuations (Figs. 8b and 9b). Noticeably larger values of $\overline{w'w'w'}$ in the upper part of the mixed layer (Fig. 9b) may be the main cause of the skewness overestimation in model studies of all kinds as compared to the atmospheric CBL. This casts doubts on the explanation of Mason (1989), who suggests that the greater values of skewness near the inversion in the modeled CBL arise from relatively low values of $\overline{w'w'}$, rather than from larger $\overline{w'w'w'}$. The temperature skewness derived from the atmospheric measurements, Fig. 10b, slowly decays with height over the bulk of the CBL. In the well-mixed region it is slightly smaller than the skewness obtained from the wind tunnel simulations. The distinctions between the atmospheric and wind tunnel data become large in the vicinity of inversion and above it, where the top-down factors essentially determine the regime of temperature fluctuations, see also Fig. 9a. Stronger entrainment and larger temperature variances in the atmospheric CBL provide more symmetric distribution of temperature fluctuations and thus smaller negative values of the skewness.

6. Summary and conclusions

Presented results of the laboratory study of the CBL demonstrate the possibility of using the thermally stratified wind tunnel of IHW to reproduce the main features of the turbulence regime in the atmospheric CBL, which develops under an imposed temperature inversion.

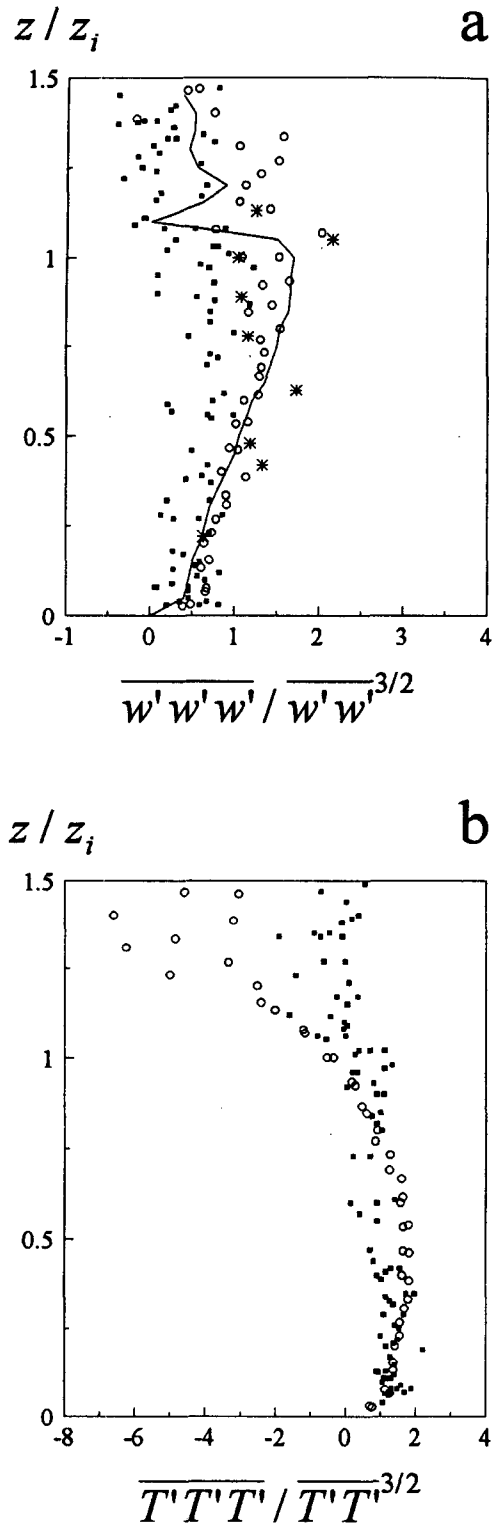

FIG. 10. (a) Vertical velocity and (b) temperature skewness as functions of the dimensionless height. Data from the wind tunnel experiments are shown by the circles. The filled squares are atmospheric measurement results from Sorbjan (1991), asterisks are the water tank data of Deardorff and Willis (1985), and the solid line represents the LES data of Schmidt and Schumann (1989).

The modeling approach employed in the tunnel focuses on the longitudinal evolution of the CBL over a heated surface, thus, considering the growth of the convectively mixed layer due to advection-type entrainment of warmer air from upper turbulence-free layers. Most numerical and laboratory model studies of the CBL carried out so far have dealt with nonsteady entrainment, when the CBL growth is a nonstationary process. In the atmosphere both types of the CBL development can take place, either separately, or in conjunction. The comparison of the turbulence statistics, derived from the wind tunnel measurement data by the temporal averaging, with spatial averages from water tank and LES studies suggests that turbulence regimes in the nonsteady and horizontally evolving CBLs are quite similar.

Investigated flow configurations were characterized by moderate values of Richardson numbers $\mathrm{Ri}_{\Delta T}$ (<10) and Ri_N (<20), representing the effects of the temperature increment across the capping inversion and stable stratification in the turbulence-free layer, respectively. Both numbers were well within the observed atmospheric ranges, although higher values of $\mathrm{Ri}_{\Delta T}$ and Ri_N in the atmospheric CBL are not exceptional. Thus, we may claim that the CBL turbulent regimes simulated in the tunnel correspond to those observed under convective conditions in the atmosphere when neither the capping inversion nor the hydrostatic stability of the upper air are very strong.

Experimental results show that under such conditions the vertical turbulent exchange in the CBL is mainly determined by bottom-up forcings, which are convective heat transfer and shear at the underlying surface. The entrainment and associated negative heat flux across the entrainment zone are weak. Still, noticeable regions with negative Q values exist close to the top of the CBL. Intensive convective mixing achieved in the wind tunnel flow provides constancy with height of the heating rate, which results in linear heat flux profiles within the main portion of the simulated CBL.

Modest, if expressed in nondimensional form, inversion strength in the simulated CBL is the main reason for the smallness of temperature fluctuations in the upper part of the CBL as compared with data from studies with larger $\mathrm{Ri}_{\Delta T}$. For the same reason, the horizontal velocity variance in the wind tunnel experiments displays almost monotonous decay within the inversion layer, with merely a slight bend in the profile. Theoretical and laboratory model studies with stronger inversions indicate that pronounced maximums in the profiles of both temperature and horizontal velocity variances in the vicinity of the inversion appear when heat is transported downward within a comparatively thin entrainment layer with large temperature difference across it and when sideward motions in the upper part of the CBL are generated as a result of the updrafts breaking at the sharp density interface.

The surface shear was found to be an essential contributor to the turbulence production in the simulated CBL. Values of the bottom-up buoyancy/shear ratio u_*/w_* of about 0.3 resulted in a noticeable increase of velocity components variances in the lower portion of the layer compared with the shear-free CBL.

Another mechanism of the velocity fluctuations enhancement, which mostly affects the vertical component variance in the middle part of the layer, is associated with semiorganized quasi-steady motions relevant to weak roll-like circulations in the tunnel. Additional experiments, incorporating high-resolution mean-velocity and turbulence measurements over planes transversal to the tunnel flow, are needed to better understand the interaction between the low-frequency coherent structures and higher-frequency turbulence components, which both contribute to the exchange processes in the simulated CBL. Also quite useful from this point of view could be measurements of the turbulence spectra in the tunnel, which we consider as the most important next step of the wind tunnel studies on simulating turbulent flow in the atmospheric CBL.

Acknowledgments. The reported wind tunnel study was a part of the IHW contribution to Sonderforschungsbereich 210, funded by the German Science Foundation (DFG). The authors are thankful to Ulrich Schumann for his useful remarks and for providing the LES data. The first author gratefully acknowledges support from the Alexander von Humboldt Foundation.

APPENDIX

Derivation of the Momentum, Heat, and TKE Integral Balance Equations

A zero-order jump parameterization of the CBL vertical structure is based on the fact that heat and momentum are well mixed within the bulk of the layer, and significant changes in the temperature and velocity profiles are confined to comparatively shallow surface and interfacial layers (Zilitinkevich 1991). In this way, the CBL can be represented by the mixed layer with two interfaces, the upper one (at $z = z_i$) and the lower one (at $z = 0$), across which temperature and velocity change in a jumplike way. The vertical structure of the velocity and temperature fields above CBL, in the turbulence-free layer, is assumed to be known.

To describe the two-dimensional flow in a quasi-stationary, horizontally nonhomogeneous boundary layer, where advection and vertical turbulent exchange are determining processes, the following equations in the Reynolds form can be used.

The momentum balance equation is

$$\frac{\partial uu}{\partial x} + \frac{\partial wu}{\partial z} = -\frac{1}{\rho_0}\frac{\partial p}{\partial x} + \frac{\partial \tau}{\partial z}, \qquad \text{(A1)}$$

where p is the pressure and ρ_0 is the reference density. It is assumed that hydrostatic equilibrium is satisfied in the CBL, which implies $(1/\rho_0)(\partial p/\partial z) = \beta T$. No external pressure forcing affects the flow in the tunnel, and thus the horizontal pressure gradient in the CBL may be associated solely with the longitudinal changes of the flow temperature (Qi et al. 1994).

The mass conservation equation is

$$\frac{\partial u}{\partial x} + \frac{\partial w}{\partial z} = 0, \qquad \text{(A2)}$$

and the heat transfer equation is given by

$$\frac{\partial uT}{\partial x} + \frac{\partial wT}{\partial z} = -\frac{\partial Q}{\partial z}. \qquad \text{(A3)}$$

Employing the zero-order jump parameterizations for the velocity and temperature profiles, integral forms of the momentum and heat balance equations can be obtained. Integrating each term of the equation of motion (A1) from 0 to z_{i+} (the upper side of the zero-order discontinuity surface representing the interfacial layer), using the rule of differentiating integrals with variable limits [since in our case $z_i = z_i(x)$], taking into account the zero-order jump representation of the velocity profile ($u = 0$ at $z = 0$, $\tau = 0$ at $z > z_i$, $\overline{\overline{uu}} = \overline{\overline{u}}^2$), substituting w_{z_i} from the integrated continuity equation (A2) with boundary condition $w = 0$ at $z = 0$, expressing the pressure gradient integral through the averaged CBL temperature variation, using the hydrostatic equation, and neglecting horizontal pressure changes at the inversion level, we come to (1) of section 4.

A similar integration procedure applied to the heat balance equation (A3) gives (2) of section 4, which is the expression of the integral budget of heat in the simulated CBL.

The model representations of the momentum and heat flux profiles, (3) and (4) of section 4, respectively, are obtained by integrating (A1) and (A3) over the vertical coordinate from 0 to $z < z_i$, employing the zero-order jump parameterizations of the velocity and temperature profiles, calculating $w(z)$ and $p(z)$ from the continuity and hydrostatic equations, respectively, and using expressions of integral budgets of momentum and heat, (1) and (2).

The TKE balance equation in the case studied has the form

$$\frac{\partial ue}{\partial x} + \frac{\partial we}{\partial z} = \tau\frac{\partial u}{\partial z} + \beta Q - \frac{\partial \Phi}{\partial z} - \epsilon, \qquad \text{(A4)}$$

where e is the turbulence kinetic energy per unit mass, ϵ is its dissipation rate, and Φ is the vertical transport of kinetic energy due to turbulent exchange and pressure fluctuations.

Equation (5) of section 4 presenting the TKE integral budget in the simulated CBL can be obtained from (A4) by its termwise integration over z from 0 to z_{i+}.

The integration of the shear production term in the right-hand part of (A4) cannot be carried out directly

because we have to integrate the product of the shear stress component, (which is discontinuous at $z = z_i$) and the vertical derivative of the horizontal velocity component (it is infinite at $z = 0$ and $z = z_i$ according to the parameterization used). To overcome this difficulty, we approximate differentials in the vicinity of z_i by finite differences over a layer with depth $\delta z_i = z_{i+} - z_{i-}$. Then, for the velocity gradient across δz_i, we have $\Delta u/\delta z_i$, and the increment of the shear stress can be represented by the linear function $\Delta u(d\bar{\bar{u}}z_i/dx)(z_{i+} - z/\delta z_i)$. Multiplication of these two terms, and integration of the product over δz_i, yields $\frac{1}{2}\Delta u^2(d\bar{\bar{u}}z_i/dx)$, the value of the integral being independent on δz_i. Therefore, it holds true when δz_i tends to zero. Calculating the integral over the rest of the mixed layer, we should take into account that in the bulk of the layer the velocity is assumed to be height constant, and therefore there is no shear production of turbulent kinetic energy in this region. The contribution of the shear in the thin near-surface layer, where velocity sharply increases from zero to the value characteristic of the mixed layer and shear stress variation with height is negligibly small, can be evaluated in the way analogous to that used in the vicinity of z_i. Such integration results in $\bar{\bar{u}}\tau_s$.

Integrating the other terms of (A4), taking into account that $e = 0$ at $z = z_{i+}$ (there is no turbulence above the inversion according to the zero-order jump model) and that energy is not transported through the underlying surface, we obtain (5).

REFERENCES

Adrian, R. J., R. T. D. S. Ferreira, and T. Boberg, 1986: Turbulent thermal convection in wide horizontal fluid layers. *Experiments in Fluids,* Vol. 4, Springer-Verlag, 121–141.

Ball, F. K., 1960: Control of inversion height by surface heating. *Quart. J. Roy. Meteor. Soc.,* **86,** 483–494.

Carson, D. J., and F. B. Smith, 1974: Thermodynamic model for the development of a convectively unstable boundary layer. *Advances in Geophysics,* Vol. 18A, Academic Press, 111–124.

Caughey, S. J., and S. G. Palmer, 1979: Some aspects of turbulence structure through the depth of the convective boundary layer. *Quart. J. Roy. Meteor. Soc.,* **105,** 811–827.

Cenedese, A., and G. Querzoli, 1994: A laboratory model of turbulent convection in the atmospheric boundary layer. *Atmos. Environ.,* **28,** 1901–1914.

Clarke, R. H., A. J. Dyer, R. R. Brook, D. G. Reid, and A. J. Troup, 1971: The Wangara experiment: Boundary layer data. Tech. Paper 19, Div. Meteor. Phys., CSIRO Australia, 363 pp. [NTIS N71-37838.]

Coleman, G. N., J. H. Ferziger, and P. R. Spalart, 1994: A numerical study of the convective boundary layer. *Bound.-Layer Meteor.,* **70,** 247–272.

Deardorff, J. W., 1970: Convective velocity and temperature scales for the unstable planetary boundary layer and for Raleigh convection. *J. Atmos. Sci.,* **27,** 1211–1213.

——, and G. E. Willis, 1985: Further results from a laboratory model of the convective planetary boundary layer. *Bound.-Layer Meteor.,* **32,** 205–236.

——, ——, and D. K. Lilly, 1969: Laboratory investigation of nonsteady penetrative convection. *J. Fluid Mech.,* **35,** 7–31.

——, ——, and B. H. Stockton, 1980: Laboratory studies of the entrainment zone of a convectively mixed layer. *J. Fluid Mech.,* **100,** 41–64.

Fedorovich, E. E., and D. V. Mironov, 1995: A model for a shear-free convective boundary layer with parameterized capping inversion structure. *J. Atmos. Sci.,* **52,** 83–95.

——, R. Kaiser, and M. Rau, 1995: Simulation of convective boundary layer turbulence structure in the thermally stratified wind tunnel. *Proc. 11th Symp. on Boundary Layers and Turbulence,* Charlotte, NC, Amer. Meteor. Soc., 544–547.

Holtslag, A. A. M., and F. T. M. Nieuwstadt, 1986: Scaling the atmospheric boundary layer. *Bound.-Layer Meteor.,* **36,** 201–209.

Hooper, W. P., and E. W. Eloranta, 1986: Lidar measurements of wind in the planetary boundary layer: The method, accuracy and results from joint measurements with radiosonde and kytoon. *J. Climate Appl. Meteor.,* **25,** 990–1001.

Kaimal, J. C., J. C. Wyngaard, D. A. Haugen, O. R. Coté, Y. Izumi, S. J. Caughey, and C. J. Readings, 1976: Turbulence structure in a convective boundary layer. *J. Atmos. Sci.,* **33,** 2152–2169.

Kantha, L. H., 1977: Note on the role of internal waves in thermocline erosion. *Modelling and Predictions of the Upper Layer of the Ocean,* E. B. Kraus, Ed., Pergamon, 173–177.

Kumar, R., and R. J. Adrian, 1986: Higher order moments in the entrainment zone of turbulent penetrative thermal convection. *J. Heat Trans.,* **108,** 323–329.

Lenschow, D. H., and P. L. Stephens, 1980: The role of thermals in the convective boundary layer. *Bound.-Layer Meteor.,* **19,** 509–532.

——, J. C. Wyngaard, and W. T. Pennel, 1980: Mean-field and second-momentum budgets in a baroclinic, convective boundary layer. *J. Atmos. Sci.,* **37,** 1313–1326.

Lilly, D. K., 1968: Models of cloud-topped mixed layers under a strong inversion. *Quart. J. Roy. Meteor. Soc.,* **94,** 292–309.

Mason, P. J., 1989: Large-eddy simulation of the convective atmospheric boundary layer. *J. Atmos. Sci.,* **46,** 1492–1516.

Meroney, R. N., and W. H. Melbourne, 1992: Operating ranges of meteorological wind tunnels for the simulation of convective boundary layer (CBL) phenomena. *Bound.-Layer Meteor.,* **61,** 145–174.

Moeng, C.-H., 1984: A large-eddy simulation for the study of planetary boundary layer turbulence. *J. Atmos. Sci.,* **41,** 2052–2062.

Nelson, E., R. Stull, and E. Eloranta, 1989: A prognostic relationship for entrainment zone thickness. *J. Appl. Meteor.,* **28,** 885–903.

Ogawa, Y., P. G. Diosey, K. Uehara, and H. Ueda, 1981: A wind tunnel for studying the effects of thermal stratification in the atmosphere. *Atmos. Environ.,* **15,** 807–821.

Poreh, M., and J. Cermak, 1984: Wind tunnel simulation of diffusion in a convective boundary layer. *Bound.-Layer Meteor.,* **30,** 431–455.

——, M. Rau, and E. Plate, 1991: Design considerations for wind tunnel simulations of diffusion within the convective boundary layer. *Atmos. Environ.,* **25A,** 1250–1257.

Qi, Y., J. Zhou, and B. Fu, 1994: Airflow over a mountain and the convective boundary layer. *Bound.-Layer Meteor.,* **68,** 301–318.

Rau, M., and E. Plate, 1995: Wind tunnel modelling of convective boundary layers. *Wind Climate in Cities,* J. Cermak, A. G. Davenport, E. J. Plate, and D. X. Vigas, Eds., Kluwer, 431–456.

——, W. Bächlin, and E. Plate, 1991: Detailed design features of a new wind tunnel for studying the effects of thermal stratification. *Atmos. Environ.,* **25A,** 1258–1263.

Rey, C., J. P. Schon, and J. Mathieu, 1979: Buoyancy effects in a wind tunnel simulation of the atmospheric boundary layer. *Phys. Fluids,* **22,** 1020–1028.

Schmidt, H., and U. Schumann, 1989: Coherent structures of the convective boundary layer derived from large-eddy simulations. *J. Fluid Mech.*, **200,** 511–562.

Sorbjan, Z., 1990: Similarity scales and universal profiles of statistical moments in the convective boundary layer. *J. Appl. Meteor.*, **29,** 762–775.

——, 1991: Evaluation of local similarity functions in the convective boundary layer. *J. Appl. Meteor.*, **30,** 1565–1583.

Stull, R. B., 1988: *An Introduction to Boundary Layer Meteorology.* Kluwer, 666 pp.

Thorpe, S. A., 1973: Turbulence in stably stratified fluids: A review of laboratory experiments. *Bound.-Layer Meteor.*, **5,** 95–119.

Willis, G. E., and J. W. Deardorff, 1974: A laboratory model of the unstable planetary boundary layer. *J. Atmos. Sci.*, **31,** 1297–1307.

——, and ——, 1976: On the use of Taylor's translation hypothesis for diffusion in the mixed layer. *Quart. J. Roy. Meteor. Soc.*, **102,** 817–822.

Wyngaard, J. C., 1992: Atmospheric turbulence. *Annu. Rev. Fluid Mech.*, **24,** 205–233.

——, and R. A. Brost, 1984: Top-down and bottom-up diffusion of a scalar in the convective boundary layer. *J. Atmos. Sci.*, **41,** 102–112.

Zilitinkevich, S. S., 1991: *Turbulent Penetrative Convection.* Avebury Technical, 179 pp.